10.2 A NUMERICAL INVESTIGATION OF THE EFFECTS OF DRY AIR ALOFT ON QUASI-LINEAR CONVECTIVE SYSTEMS

Richard P. James* and Paul M. Markowski
The Pennsylvania State University, University Park, Pennsylvania

1. INTRODUCTION

The influence of environmental properties on the characteristics of deep convection has been a fruitful area of research for many years. Environmental parameters known to have important effects on convection include wind shear, CAPE and convective inhibition. The relative humidity of the convective environment above cloud base is also widely regarded as having significance for convective processes, but differing opinions are found in the literature concerning the precise role of environmental humidity.

Beginning with early observational studies on severe convective storms, dry air aloft has generally been regarded as favorable for the generation of cold downdrafts and stronger low-level outflow (e.g. Newton 1950, Browning and Ludlam 1962). In the severe storms forecasting literature, low humidity aloft has been described as an ingredient for severe straight-line winds (Johns and Hirt 1987). This interpretation was supported by the modeling results of Gilmore and Wicker (1998), who found that low-level outflow from supercells was more vigorous when the relative humidity was reduced between approximately 2 and 4 km above ground level (AGL). However, observational and modeling results from studies of convection over the tropical oceans have documented that dry air above cloud base can have strongly detrimental effects on convection (e.g. Brown and Zhang 1997, Lucas et al. 2000).

In view of the surprising variety of effects assigned to dry air in the literature, a modeling study was undertaken to develop a better understanding of the role of the environmental humidity. Section 2 describes the modeling framework, Section 3 presents the primary results, and the improved conceptual understanding is outlined in Section 4.

2. METHODOLOGY

The numerical model of Bryan and Fritsch (2002) and Bryan (2002) was used to investigate the sensitivity of simulated quasi-linear convective systems to the relative humidity above cloud base. The model was configured to solve the compressible equations in a three-dimensional framework, using a horizontally homogeneous base state into which a line of warm, moist bubbles was introduced at the initial time. The horizontal grid spacing was 400 m, and the vertical grid spacing was 250 m. The size of the domain was 400 km in the across-line direction, with an open-radiative boundary condition, and 80 km in the along-line direction, with a periodic boundary condition. Free-slip lower and upper boundary conditions were used, and the simulations were run out to six hours.

The physics routines employed in the simulations included a subgrid turbulence parameterization based on the turbulence kinetic energy scheme of Deardorff (1980), and the NASA-Goddard version of the Lin et al. (1983) microphysics scheme, which represents five hydrometeor species including snow and hail. Surface fluxes and radiative effects were excluded, as was the Coriolis force.

Model base states were constructed using the technique of James et al. (2006), with CAPE varying from 3000 J kg^{-1} to 4500 J kg^{-1}. The mixing layer was 1125 m deep, with a relative humidity of 95 % at its top. In the control simulations, the relative humidity decreased steadily to 50 % at the tropopause, representing a moist but unsaturated environment. The effects of varying midlevel humidity were then investigated by introducing a layer spanning seven model levels (1.75 km) in which the relative humidity was reduced to 10 %. The height of the center of the dry layer varied from 2.625 km AGL to 4.125 km AGL. In the base states containing a dry layer, the temperature profile was adjusted to conserve the virtual temperature profile, so that the vertical distribution of buoyancy and the CAPE were identical to those in the control simulations. A pair of soundings is illustrated in Fig. 1.

The base state wind profile was designed with constant wind shear perpendicular to the convective line in the lowest 2.5 km, and zero wind shear elsewhere. For soundings with CAPE of 4000 J kg^{-1} or higher, the magnitude of the shear was 17.5 m s^{-1} over 2.5 km, but the shear was reduced to 10 m s^{-1} for simulations with CAPE of 3000 J kg^{-1} in order to favor an upshear-tilted convective mode.

3. RESULTS

3.1 *Sensitivity of system strength*

All of the control simulations with a relatively moist environment exhibited long-lived, vigorous convective systems consisting of a quasi-linear region of deep convective updrafts and downdrafts oriented

* *Corresponding author address*: Richard P. James, Department of Meteorology, 503 Walker Building, University Park, PA 16802; e-mail: rpj105@earthlink.net

perpendicular to the wind shear, and a trailing stratiform region that expanded rearwards in a shear-relative sense. The influence of environmental dry air is illustrated using a pair of simulations having CAPE of 4000 J kg^{-1}; in the modified base state, the dry layer was centered at 3.375 km AGL. In the presence of dry air, the total condensation and total rainfall were reduced (Fig. 2) and the domain-wide maximum vertical velocity in both the upwards and downwards directions was diminished (Fig. 3). These changes occurred owing to the entrainment of drier air into the convective updrafts, which reduced both the positive buoyancy and the water vapor content of the updrafts; this process is illustrated in Fig. 4. At the model's lowest level (125 m above ground), the domain-wide minimum potential temperature perturbation was largely unchanged (Fig. 5).

A more robust measure of the strength of the low-level cold pool is the parameter C^2 (Weisman 1992), which is proportional to the integrated negative buoyancy perturbation through the depth of the cold pool:

$$C^2 = -2g \int_0^D \frac{\theta_\rho - \theta_{\rho 0}}{\theta_{\rho 0}} dz \quad (1)$$

where g is the acceleration due to gravity, D is the depth of the cold pool as defined by the upper limit of the -1 K potential temperature perturbation, θ_ρ is the density potential temperature (Emanuel 1994) and $\theta_{\rho 0}$ is the base state density potential temperature. C is shown in Fig. 6 for the pair of squall line simulations at 4 hours, when the systems were in their mature phase. The horizontal structure of the integrated cold pool strength was similar in the two systems, but C was slightly greater in the leading portion of the cold pool in the simulation with a moist troposphere.

The detrimental effects of midlevel dry air on system strength were much greater when CAPE was less. Using a base state with CAPE of 3000 J kg^{-1}, a more dramatic difference was observed between the convection with and without the 1.75 km-deep dry layer. As shown in Fig. 7, reduced environmental humidity caused the total condensation and total rainfall to be substantially reduced; the cold pool strength was also markedly reduced (Fig. 8). In contrast, when the CAPE was increased to 4500 J kg^{-1}, the system was hindered little by dry air, and the cold pool strength was largely unchanged (not shown).

Dry air aloft was found to exert greater effects on system strength when the dry layer was located at lower elevation. Figure 9 illustrates the difference between convective systems at very high CAPE (4500 J kg^{-1}) that were simulated with dry layers centered at heights of 2.625 km AGL, 3.375 km AGL, and 4.125 km AGL. In the latter case, the convection was hindered relatively little, but when the dry layer was located just above cloud base, the inhibition of the convection was greater.

3.2 *Sensitivity of downdraft processes*

The simulated effects of dry air aloft on the formation and intensification of cold downdrafts are of particular interest in view of the oft-emphasized role of dry air in promoting severe low-level outflow winds. As shown in Figs. 6 and 8, the cold pool strength in the simulated convective systems was not enhanced in the presence of dry air; in contrast, the cold pool was weakened by a drier environment in all simulations except those at very high CAPE. The mechanisms responsible for this surprising result were examined using trajectory data.

Backwards trajectories were calculated over a 30-minute time interval prior to 4 hours in both the moist and dry simulations with CAPE of 4500 J kg^{-1}, in order to determine the history of the parcels that comprised the cold pool at 4 hours. Trajectories were initialized at every grid point on the 10 lowest model levels (up to 2.375 km AGL) over a horizontal region spanning the entire domain in the along-line direction and extending for 100 km in the across-line direction. A number of derived fields such as buoyancy and relative humidity were interpolated to the trajectory locations at every time step for diagnostic purposes. For ease of interpretation, the trajectory data were subsequently averaged in the along-line direction with respect to their position relative to the gust front at the initialization time.

The 30-minute vertical displacement of trajectories ending at 1.125 km AGL is shown in Fig. 10 for the simulations with and without a dry layer. Two distinct regions of significant downdraft formation were present in both simulations. The downdraft region closer to the gust front was coincident with the zones of maximum along-line averaged rain evaporation and hail melting, while the downdrafts further behind the gust front were associated with snow melting, snow sublimation and rain evaporation at the rear of the expanding stratiform region (Fig. 11). The along-line averaged vertical displacement of downdraft parcels was slightly greater in both regions in the presence of dry air. The virtual potential temperature perturbation was slightly more negative in the rearmost downdraft region, but was almost unchanged elsewhere (Fig. 12).

The absence of substantially enhanced cooling within the downdraft regions in the presence of dry air is consistent with the simulated rates of latent cooling from water condensate phase changes. In the drier environment, rain evaporation rates were slightly enhanced in both downdraft regions, but hail melting, which contributes significantly to the total latent cooling in the forward downdraft region, was strongly reduced. The total cooling from all evaporation and melting processes (Fig. 13) was slightly increased in the rearward region, but was almost unchanged in magnitude, and was displaced to lower elevation, in the forward region.

Further investigation reveals that the significant reduction in hail melting rates in the forward downdraft

region was attributable to reduced hail mixing ratios (Fig. 14a,b). In fact, condensate mixing ratios were universally lower in the convective system having a dry environment (Fig. 14c,d), owing to the entrainment of dry air into updrafts. The reduction in rain mixing ratios in the presence of dry air prevented the rain evaporation rate from being strongly enhanced by the lower environmental humidity. Thus the detrimental effects of dry air entrainment on total condensate production also caused the absence of significantly enhanced cooling in the presence of dry air.

The results described here for the pair of simulations with CAPE of 4500 J kg^{-1} represent the scenario in which the environmental dry layer was least detrimental to system strength and most favorable to downdraft intensification. At lower values of CAPE, dry air aloft caused greater reductions in condensate mixing ratios, and the total cooling from phase changes was reduced in the forward downdraft region. For CAPE of 3000 J kg^{-1}, the latent cooling was also reduced in the rearward downdraft region, and the low-level temperature perturbations were markedly reduced in the drier environment (not shown).

4. DISCUSSION

The model results presented here suggest a simple conceptual framework for understanding the effects of dry air aloft on deep convection. The influence of dry air above cloud base is mediated primarily by its effect on the process of entrainment into updrafts. When relatively dry air is present, the erosion of updraft buoyancy by entrainment is enhanced owing to increased evaporational cooling as environmental air is incorporated into updrafts. Moreover, the total water content within updrafts is reduced by the entrainment of lower vapor mixing ratios. These effects dampen the intensity of the updrafts and reduce the rates of production of all hydrometeor species.

Turning to the downdraft formation process, idealized numerical models have shown that lower environmental relative humidity favors stronger downdrafts, all other quantities being equal (e.g. Proctor 1989). However, the effect of dry air aloft on hydrometeor mixing ratios implies that all other quantities are not equal. The reduction of hydrometeor mixing ratios caused by dry air entrainment tends to reduce hydrometeor evaporation rates and therefore acts to offset the favorable effects of lower humidity. Moreover, in convective systems having a significant contribution to latent cooling from melting of ice particles, the rate of ice melting is not enhanced by lower humidity, but is substantially reduced by the drop in ice mixing ratios. The model results described here indicate that the overall effect of these processes is to reduce the total cooling within downdrafts in the convective region when dry air is present, except in a very high-CAPE environment, in which case the cooling is unchanged. In the downdraft region at the rear of the stratiform region, dry air aloft causes slightly enhanced cooling at high CAPE, but reduced cooling at CAPE of 3000 J kg^{-1}. The integrated cold pool strength is unchanged at very high CAPE, but reduced at lower CAPE.

The sensitivity to CAPE may be understood in terms of the fractional dilution of updrafts by entrained air. According to the entraining plume model, the increase in mass flux with height is described by:

$$\frac{dM}{dz} = \alpha M \tag{2}$$

where M is the mass flux, and α is the fractional entrainment rate, which is usually taken to be inversely proportional to the cloud radius. In a higher-CAPE environment, the average radius of convective updrafts is larger, and the updrafts tend to assume a more two-dimensional form at low levels (James et al. 2005). Consequently the fractional entrainment rate is reduced, which implies that updrafts are proportionately less affected by environmental dry air. Hydrometeor mixing ratios are thus reduced relatively little, and downdraft and cold pool strengths are not hindered.

The notion that environmental dry air may be detrimental to downdraft and cold pool strength is counter to the common perception that dry air aloft can play a significant role in promoting intense downdrafts and severe low-level outflow winds. Clearly, further testing is required to determine if and when convective storms do indeed respond to dry air with enhanced low-level outflow. However, it is possible that the role of dry air aloft has been overemphasized, having arisen as a specific interpretation of early studies on severe storm forecasting. For example, Fawbush and Miller (1954) reported a strong correlation between severe wind gusts and a “downrush temperature” calculated by moist adiabatic descent from the wet-bulb freezing level. Similarly, Foster (1958) found a modest correlation between wind gusts and a calculated downdraft speed, which was obtained by assuming saturated descent from a midlevel wet-bulb adiabat. In these and other more recent studies (e.g. Atkins and Wakimoto 1991, Cohen et al. 2007), an observed correlation between lower midlevel wet-bulb temperature (or equivalent potential temperature) and stronger outflow has been interpreted as evidence of a favorable influence of dry air on downdrafts. However, this interpretation critically assumes that variations in midlevel wet-bulb temperature are primarily attributable to variations in relative humidity. In fact, few attempts have been made to separate the influence of midlevel temperature and CAPE from the influence of midlevel relative humidity. In light of the model results reported here, it seems possible that observed correlations between lower midlevel wet-bulb temperature and stronger low-level outflow may simply reflect the well-known effect of increased CAPE on cold pool strength.

5. CONCLUSIONS

Simulations of quasi-linear convective systems using a high-resolution numerical model suggest that dry air aloft exerts detrimental effects on overall convective intensity and does not favor cold pool strength or low-level outflow intensity. In environments with very high CAPE, the influence of dry air is minimized and the convection is relatively unchanged, but at moderate values of CAPE convection is significantly hindered in a drier environment. Dry air aloft has a greater inhibiting influence when it is located just above cloud base than when it is located at higher elevation.

According to the model results, dry air aloft dilutes the updraft buoyancy and updraft water vapor content, leading to a marked reduction in total condensation and precipitation rates. The decline in hydrometeor mixing ratios exerts a negative influence on evaporation rates within the downdraft regions and offsets the favorable effect of lower humidity for evaporative cooling. Furthermore, the rate of ice melting is substantially reduced in the convective region owing to the drop in ice mixing ratios. These effects prevent any significant enhancement of latent cooling in the presence of dry air, and consequently the cold pool strength is not increased in a drier environment. In environments with CAPE less than 4500 J kg^{-1}, the detrimental effects of dry air aloft are sufficient to reduce the cold pool strength.

Further numerical investigation is needed to more extensively test the concepts discussed here and to ascertain whether the sensitivity of convection to dry air depends on the organizational mode of the convection. There is also a strong need for observational work that attempts to distinguish the influence of environmental humidity from the effects of other environmental parameters.

6. REFERENCES

Atkins, N. T., and R. M. Wakimoto, 1991: Wet microburst activity over the southeastern United States: implications for forecasting. *Wea. Forecasting*, **6,** 470-482.

Brown, R. G., and C. Zhang, 1997: Variability of midtropospheric moisture and its effects on cloud-top height distribution during TOGA COARE. *J. Atmos. Sci.*, **54,** 2760-2774.

Browning, K. A., and F. H. Ludlam, 1962: Airflow in convective storms. *Quart. J. Roy. Meteor. Soc.*, **88,** 117-135.

Bryan, G. H., 2002: An investigation of the convective region of numerically simulated squall lines. Ph.D. thesis, The Pennsylvania State University, 181 pp.

_____, and J. M. Fritsch, 2002: A benchmark simulation for moist nonhydrostatic numerical models. *Mon. Wea. Rev.*, **130,** 2917-2928.

Cohen, A. E., M. C. Coniglio, S. F. Corfidi, and S. J. Corfidi, 2007: Discrimination of mesoscale convective system environments using sounding observations. *Wea. Forecasting*, **22,** 1045-1062.

Deardorff, J. W., 1980: Stratocumulus-capped mixed layer derived from a three-dimensional model. *Bound.-Layer Meteor.*, **18,** 495-527.

Emanuel, K. A., 1994: *Atmospheric Convection.* Oxford University Press, 580 pp.

Fawbush, E. J., and R. C. Miller, 1954: A basis for forecasting peak wind gusts in non-frontal thunderstorms. *Bull. Amer. Meteor. Soc.*, **35,** 14-19.

Foster, D. S., 1958: Thunderstorm gusts compared with computed downdraft speeds. *Mon. Wea. Rev.*, **86,** 91-94.

Gilmore, M. S., and L. J. Wicker, 1998: The influence of midtropospheric dryness on supercell morphology and evolution. *Mon. Wea. Rev.*, **126,** 943-958.

James, R. P., J. M. Fritsch, and P. M. Markowski, 2005: Environmental distinctions between cellular and slabular convective lines. *Mon. Wea. Rev.*, **133,** 2669-2691.

James, R. P., P. M. Markowski, and J. M. Fritsch, 2006: Bow echo sensitivity to ambient moisture and cold pool strength. *Mon. Wea. Rev.*, **134,** 950-964.

Johns, R. H., and W. D. Hirt, 1987: Derechos: Widespread convectively induced windstorms. *Wea. Forecasting*, **2,** 32-49.

Lin, Y.-L., R. D. Farley, and H. D. Orville, 1983: Bulk parameterization of the snow field in a cloud model. *J. Appl. Meteor.*, **22,** 1065-1092.

Lucas, C., E. J. Zipser, and B. S. Ferrier, 2000: Sensitivity of tropical West Pacific oceanic squall lines to tropospheric wind and moisture profiles. *J. Atmos. Sci.*, **57,** 2351-2373.

Newton, C. W., 1950: Structure and mechanism of the prefrontal squall line. *J. Meteor.*, **7,** 210-222.

Proctor, F. H., 1989: Numerical simulations of an isolated microburst. Part II: sensitivity experiments. *J. Atmos. Sci.*, **46,** 2143-2165.

Weisman, M. L., 1992: The role of convectively generated rear-inflow jets in the evolution of long-lived mesoconvective systems. *J. Atmos. Sci.*, **49,** 1826-1847.

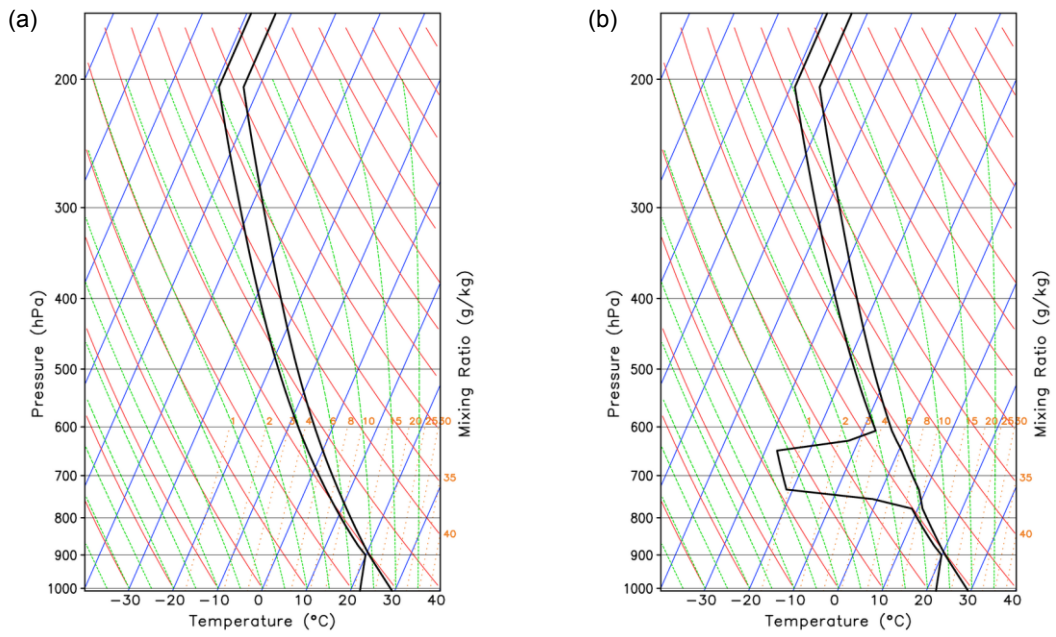

Figure 1. Base state soundings for the moist (a) and dry (b) simulations with CAPE of 4500 J kg^{-1}.

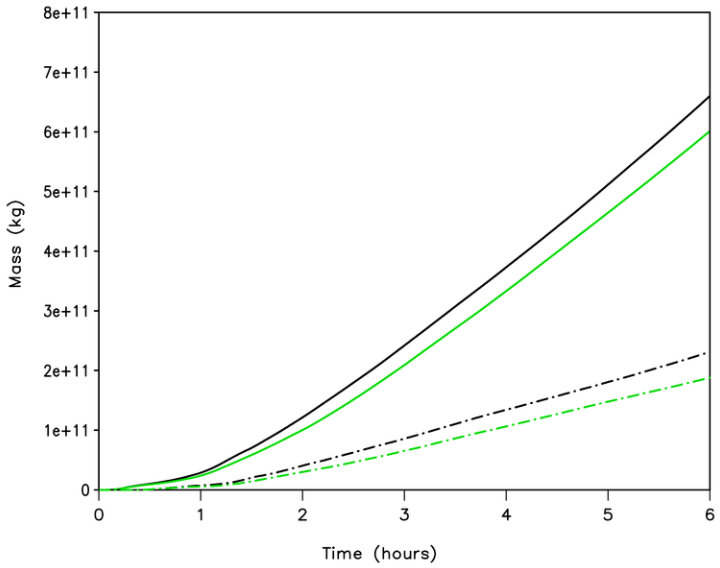

Figure 2. Total condensation (solid lines) and total rainfall (dashed lines) for the moist (black lines) and dry (green lines) simulations with CAPE of 4000 J kg^{-1}.

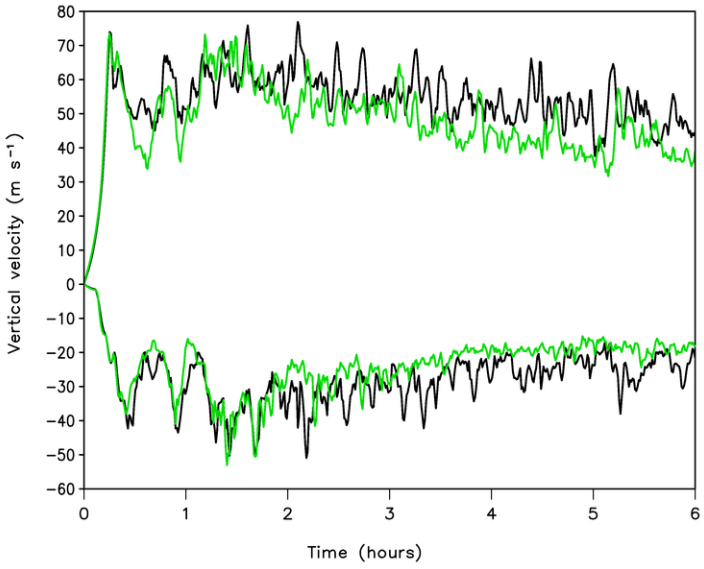

Figure 3. Domain-wide maximum (top) and minimum (bottom) vertical velocity for the moist (black lines) and dry (green lines) simulations with CAPE of 4000 J kg^{-1}.

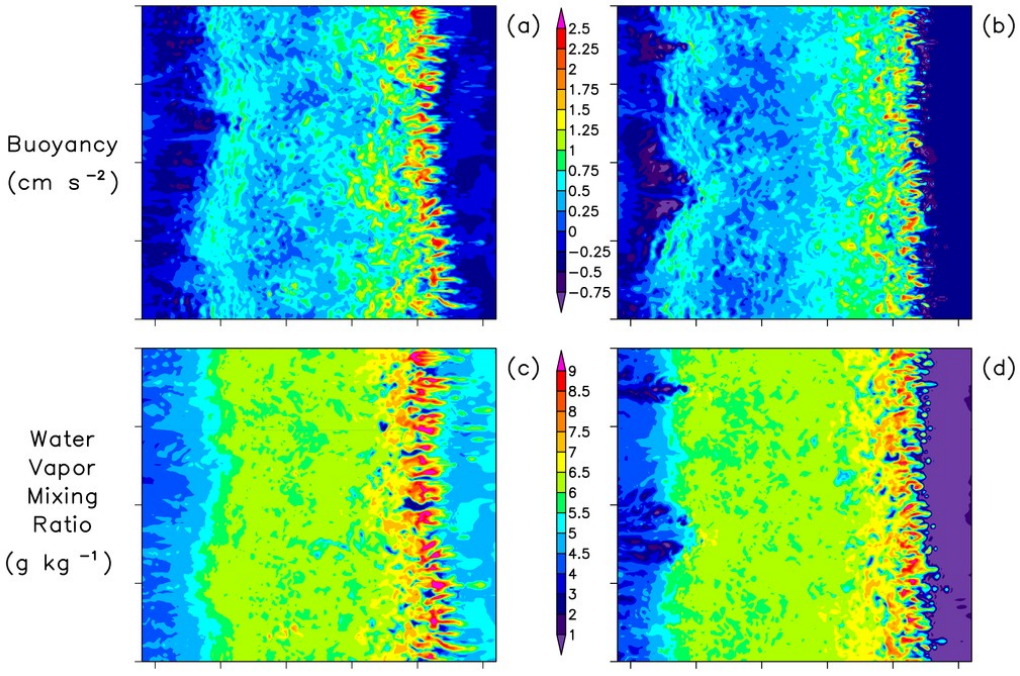

Figure 4. Buoyancy (a,b) and water vapor mixing ratio (c,d) at 4.125 km AGL at 4 hours in the moist (a,c) and dry (b,d) simulations with CAPE of 4000 J kg^{-1}. Tick marks indicate horizontal distances of 20 km.

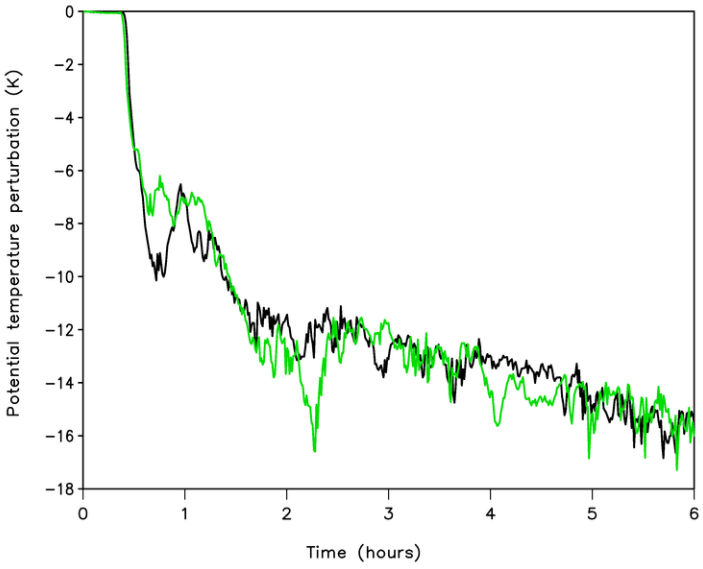

Figure 5. Domain-wide minimum potential temperature perturbation for the moist (black line) and dry (green line) simulations with CAPE of 4000 J kg^{-1}.

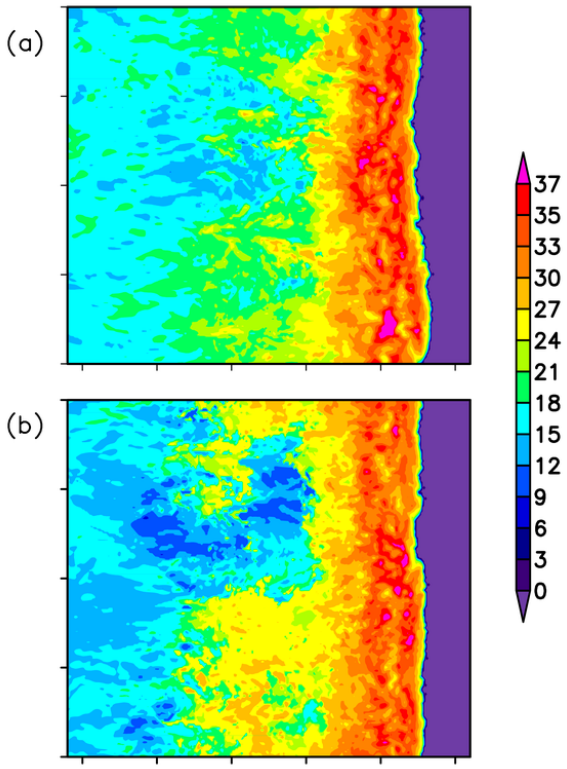

Figure 6. Integrated cold pool strength C (m s^{-1}) at 4 hours in the moist (a) and dry (b) simulations with CAPE of 4000 J kg^{-1}. Tick marks indicate horizontal distances of 20 km.

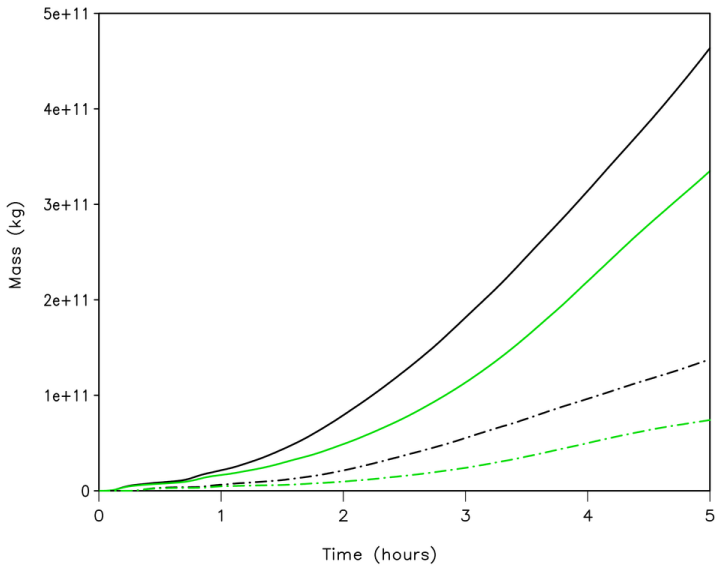

Figure 7. Total condensation (solid lines) and total rainfall (dashed lines) for the moist (black lines) and dry (green lines) simulations with CAPE of 3000 J kg^{-1}.

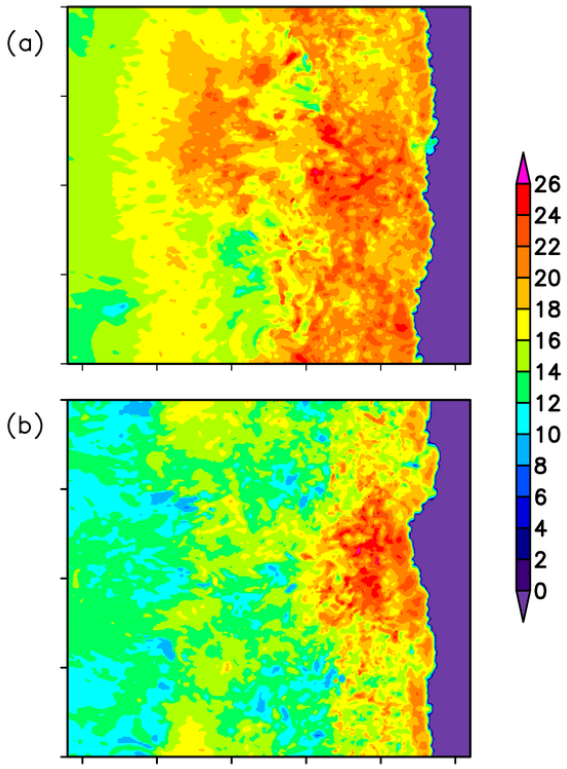

Figure 8. Integrated cold pool strength C (m s^{-1}) at 4 hours for the moist (a) and dry (b) simulations with CAPE of 3000 J kg^{-1}. Tick marks indicates horizontal distances of 20 km.

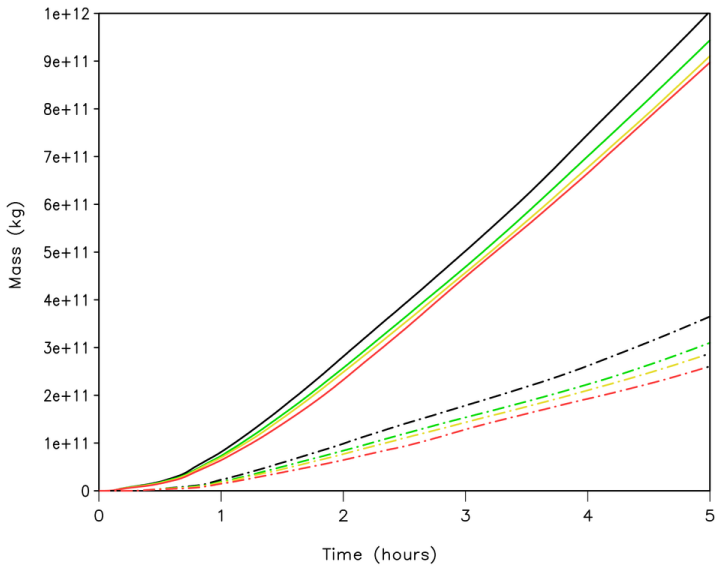

Figure 9. Total condensation (solid lines) and total rainfall (dashed lines) for moist (black) and simulations having a dry layer centered at 4.125 km AGL (green), 3.375 km AGL (yellow) and 2.625 km AGL (red) with CAPE of 4500 J kg^{-1}.

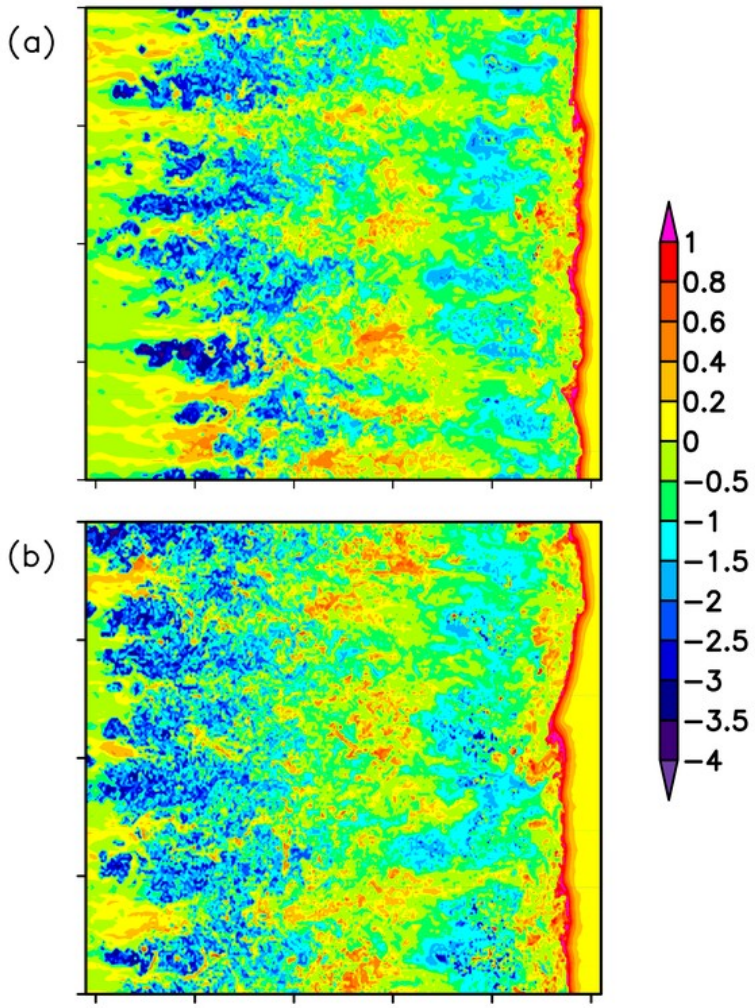

Figure 10. 30-minute vertical displacement (km) of trajectories ending at 1.125 km AGL at 4 hours in the moist (a) and dry (b) simulations with CAPE of 4500 J kg^{-1}. Tick marks indicate horizontal distances of 20 km.

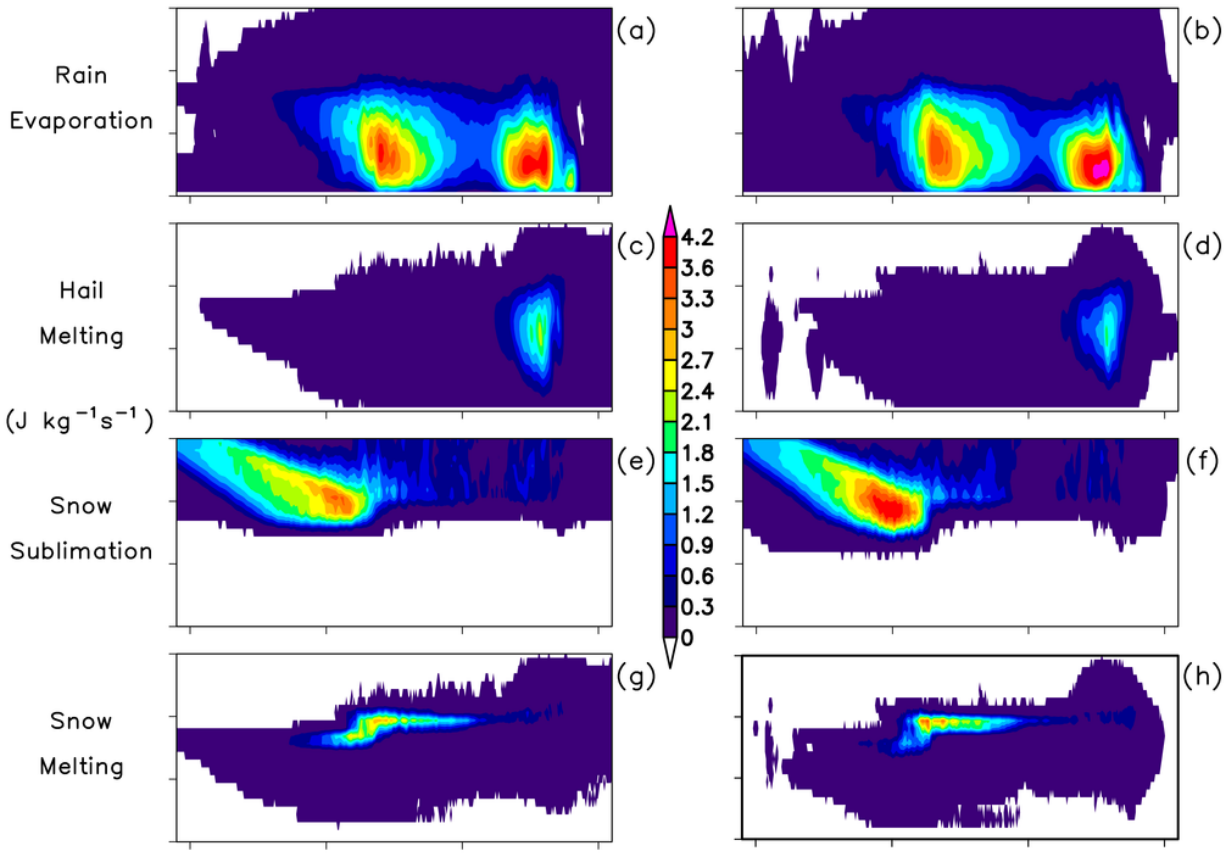

Figure 11. Rates of latent cooling from phase changes at 4 hours in the moist (a,c,e,g) and dry (b,d,f,h) simulations with CAPE of 4500 J kg^{-1}. Tick marks indicate distances of 50 km in the horizontal direction and 2 km in the vertical direction.

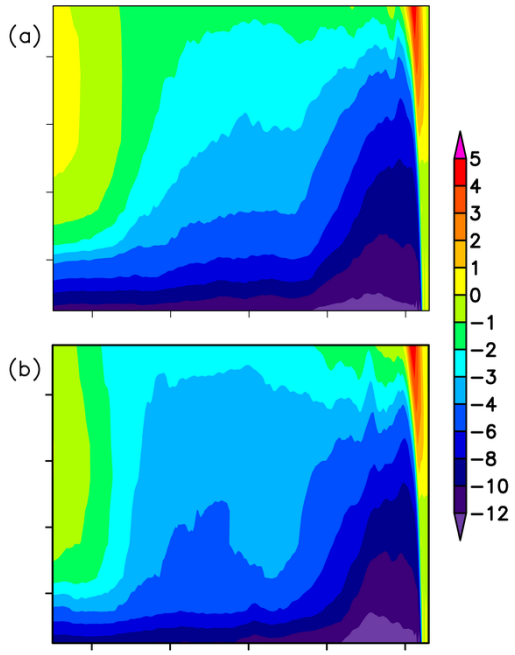

Figure 12. Along-line averaged virtual potential temperature perturbation (K) at trajectory locations at 4 hours in the moist (a) and dry (b) simulations with CAPE of 4500 J kg^{-1}. Tick marks indicate distances of 20 km in the horizontal direction and 0.5 km in the vertical direction.

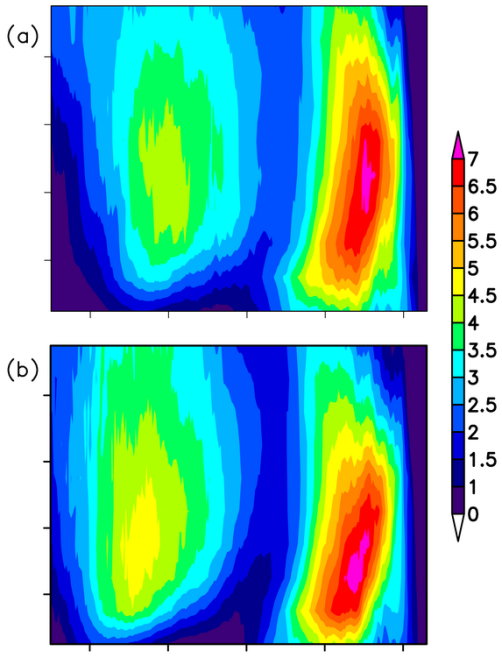

Figure 13. Along-line averaged total latent cooling (kJ kg^{-1}) from phase changes over 30-minute trajectory paths ending at 4 hours in the moist (a) and dry (b) simulations with CAPE of 4500 J kg^{-1}. Tick marks indicate distances of 20 km in the horizontal direction and 0.5 km in the vertical direction.

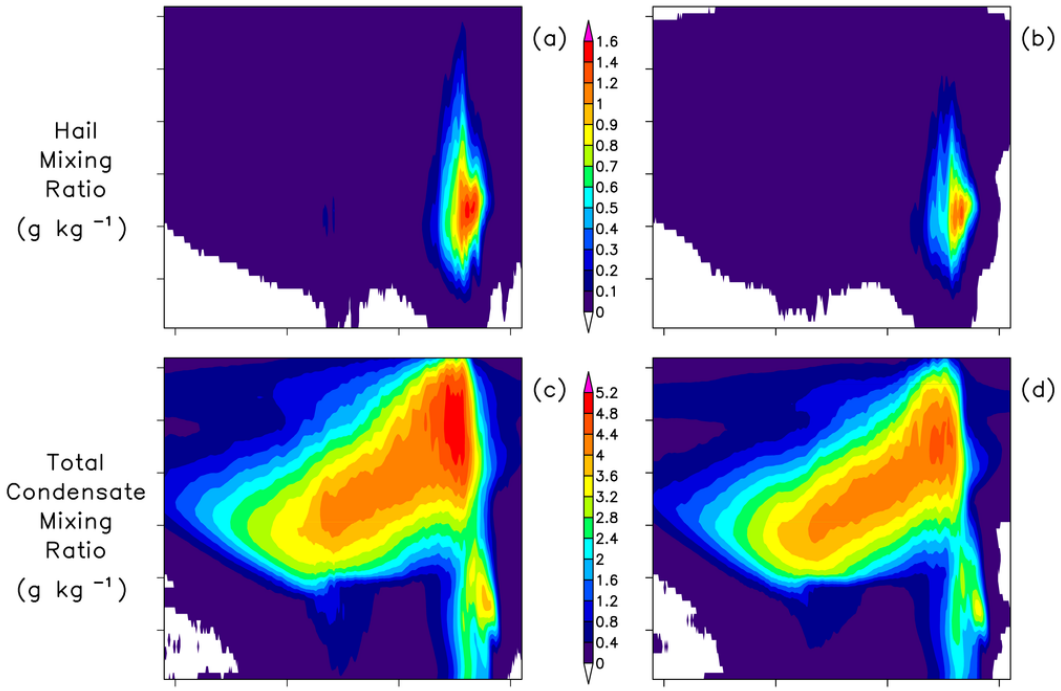

Figure 14. Along-line averaged hail mixing ratio (a,b) and total condensate mixing ratio (c,d) at 4 hours in the moist (a,c) and dry (b,d) simulations with CAPE of 4500 J kg^{-1}. Tick marks indicate distances of 50 km in the horizontal direction and 2 km in the vertical direction.